Electronic Supplementary Material (ESI) for Nanoscale.
This journal is © The Royal Society of Chemistry 2014

**Supporting Information**

# Facile Synthesis of One-dimensional $Mn_3O_4/Zn_2SnO_4$ Hybrid Composites and Their High Performance as Anodes for LIBs

*Ranran Zhang, Yanyan He, Aihua Li and Liqiang Xu**

**Figure Captions:**

**Fig. S1** XRD patterns of the final products obtained in the absence or 16 mL $NH_3 \cdot H_2O$ was added in the hydrothermal process.

**Fig. S2** (a) FTIR spectrum of the as-obtained 1branched $Mn_3O_4/Zn_2SnO_4$ composites prepared at 180 °C for 24 h (8 mL $NH_3 \cdot H_2O$); (b) Typical $N_2$ gas adsorption desorption isotherm of $Mn_3O_4/Zn_2SnO_4$ nanostructures. The inset shows the corresponding pore-size distribution curve of the product.

**Fig. S3** (a) The corresponding SAED pattern of $Zn_2SnO_4$ nanoneedle in the square area in Fig. 4c. (b) EDX spectrum of the final products (inset show the related data).

**Fig. S4** FESEM images of (a, c) branched MnOOH and as–prepared β-$MnO_2$ nanorods, respectively; (b, d) TEM images of the as-obtained MnOOH and β-$MnO_2$ nanorods, respectively.

**Fig. S5** (a, b) TEM images of $Mn_3O_4/Zn_2SnO_4$/Li after 10 cycles at a current density of 1000 mA $g^{-1}$

**Fig. S6** XRD patterns of the 1D $Mn_3O_4/ZnFe_2O_4$ nanocompositesobtained after the hydrothermal process.

**Fig. S7** TEM images of the as-obtained 1D $Mn_3O_4$ /$ZnFe_2O_4$composites at 180°C/24 h using different amounts of urea: (a) 1.7 g, (b) 1.8 g, (c)1.9 g, and (d) 2.0 g.

**Fig. S8** XRD patterns of (a) the black intermediate; (b) 1D $Mn_2O_3$/$CoFe_2O_4$ composites obtained after annealed at 620 °C in air for 2.5 h.

**Fig. S9** (a, b) TEM images ofthe black intermediate prepared at 180 °C for 24 h (8 mL$NH_3 \cdot H_2O$); (c, d) TEM image of 1D $Mn_2O_3$/$CoFe_2O_4$ composites obtained after annealed at 620 °C in air for 2.5 h.

**Fig. S10** XRD patterns of (a) the black intermediate（180 °C/24 h）; (b) 1D $Mn_2O_3$/$NiFe_2O_4$composites obtained after annealed at 680 °C in air for 2.5h.

**Fig. S11** (a, b) TEM images ofthe black intermediate prepared at 180 °C for 36 h (8 mL$NH_3 \cdot H_2O$); (c, d) TEM image of 1D $Mn_2O_3$/$NiFe_2O_4$composites obtained after annealed at 620 °C in air for 2.5 h.

**Tab. S1** Cycle performance comparisons between the $Mn_3O_4$/$ZnFe_2O_4$ composites and previously reported $ZnFe_2O_4$ structures.

**Tab. S2** Cycle performance comparisons between the $Mn_2O_3$/$CoFe_2O_4$ composites and previously reported $ZnFe_2O_4$ structures.

## Experimental Section

### *Preparation of the $Mn_3O_4/Zn_2Fe_2O_4$ hybrid composites*

The synthesis of 1D $ZnFe_2O_4/Mn_3O_4$ nanocomposites was started from the β-$MnO_2$ nanorods (prepared by annealing MnOOH nanorods at 300 °C for 4 h). The as-prepared β-$MnO_2$ nanorods (400 mg) with 25 mL deionized water were firstly ultrasonicated for 30 min and then were stirred for another 30 min. Then, 0.2 M $ZnCl_2$ (5 mL) and 0.4 M $FeCl_3·6H_2O$ (5 mL) were added into the above solution. After it is stirred for 30 min, 1.8 g urea (dissolved in 5 mL deionized water) were dropped slowly. Last, the mixed solution was continually stirred for 1h before transferred into a Teflon-lined autoclave with a capacity of 60 mL. The autoclave was heated from room temperature to 180 °C and maintained at 180 °C for 24 h. The resulting 1D $Mn_3O_4/ZnFe_2O_4$ product was collected by centrifugation and washed repeatedly with anhydrous ethanol and distilled water for several times. Finally, it was dried in vacuum at 60°C for 12 h.

### *Preparation of the $Mn_2O_3/CoFe_2O_4$ hybrid composites*

The synthesis of 1D $Mn_2O_3/CoFe_2O_4$ nanocomposites was started from the β-$MnO_2$ nanorods (prepared by annealing MnOOH nanorods at 300 °C for 4 h). The as-prepared β-$MnO_2$ nanorods (400 mg) with 25 mL deionized water were firstly ultrasonicated for 30 min and then were stirred for another 30 min. Then, 0.2 M $C_4H_6CoO_4·4H_2O$ (5 mL) and 0.4 M $FeCl_3·6H_2O$ (5 mL) were added into the above solution. After it is stirred for 30 min, 8 mL $NH_3·H_2O$ were dropped slowly. Last, the mixed solution was continually stirred for 1h before transferred into a Teflon-lined autoclave with a capacity of 60 mL. The autoclave was heated from room temperature

to 180 °C and maintained at 180 °C for 24 h. The resulting black intermediate was collected by centrifugation and washed repeatedly with anhydrous ethanol and distilled water for several times. Finally, it was dried in vacuum at 60°C for 12 h. Then the black intermediate was annealed at 620 °C in air for 2.5 h in a tube furnace, followed by natural cooling to room temperature. The heating rate was set to 5 °C $min^{-1}$.

***Preparation of the $Mn_2O_3/NiFe_2O_4$ hybrid composites***

The synthesis of 1D $Mn_2O_3/NiFe_2O_4$ nanocomposites was started from the β-$MnO_2$ nanorods (prepared by annealing MnOOH nanorods at 300 °C for 4 h). The as-prepared β-$MnO_2$ nanorods (400 mg) with 25 mL deionized water were firstly ultrasonicated for 30 min and then were stirred for another 30 min. Then, 0.2 M $C_4H_6NiO_4 \cdot 4H_2O$ (5 mL) and 0.4 M $FeCl_3 \cdot 6H_2O$ (5 mL) were added into the above solution. After it is stirred for 30 min, 8 mL $NH_3 \cdot H_2O$ were dropped slowly. Last, the mixed solution was continually stirred for 1h before transferred into a Teflon-lined autoclave with a capacity of 60 mL. The autoclave was heated from room temperature to 180 °C and maintained at 180 °C for 24 h. The resulting black intermediate was collected by centrifugation and washed repeatedly with anhydrous ethanol and distilled water for several times. Finally, it was dried in vacuum at 60°C for 12 h. Then the black intermediate was annealed at 680 °C in air for 2.5 h in a tube furnace, followed by natural cooling to room temperature. The heating rate was set to 5 °C $min^{-1}$.

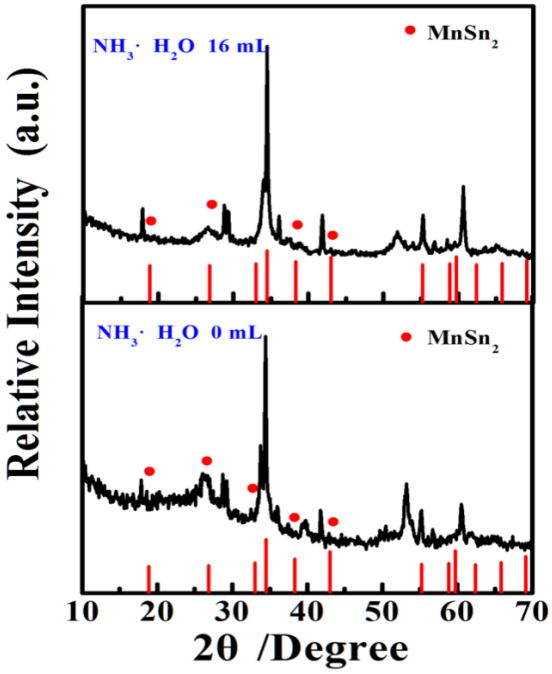


**Fig. S1** XRD patterns of the final products obtained in the absence or 16 mL $NH_3 \cdot H_2O$ was added in the hydrothermal process.

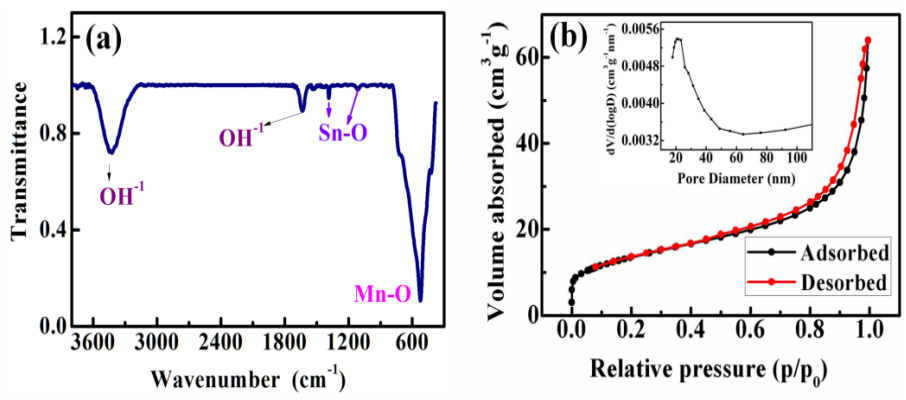


**Fig. S2** (a) FTIR spectrum of the as-obtained 1D branched $Mn_3O_4/Zn_2SnO_4$ composites prepared at 180 °C for 24 h (8 mL $NH_3 \cdot H_2O$); (b) Typical $N_2$ gas adsorption desorption isotherm of $Mn_3O_4/Zn_2SnO_4$ nanostructures. The inset shows the corresponding pore-size distribution curve of the product.

Fig. S2a shows the FTIR spectrum curve of the product. The sharp peak centered at 528 $cm^{-1}$ can be assigned to the Mn-O stretching vibration, while the bands observed at 1399 and 1113 $cm^{-1}$could be ascribed to the vibrations of the M–O or M–O–M groups in the $Zn_2SnO_4$,respectively; In addition, the bands located at 3443 and 1633 $cm^{-1}$ are attributed to the bending and stretching vibration modes of the OH group in $H_2O$, which might originate from the surface adsorption of a small amount of water in the air. Fig.S2b shows the full nitrogen sorption isotherms of the product, which gives an obvious hysteresis loop of type IV, suggesting the presence of macrospores, which may result from the mesoporous rods of the $Mn_3O_4$ and the gaps between neighboring $Zn_2SnO_4$ needle-like nanostructures. The specific surface area estimated by the Brunauer Emmett Teller (BET) method is 48.65 $m^2/g$ and as calculated by the Barrett-Joyner-Halenda (BJH) method, the size of the pores mainly centered at 22.1 nm with a relatively narrow distribution (inset in Fig. S3b), which is in the mesoporous range.

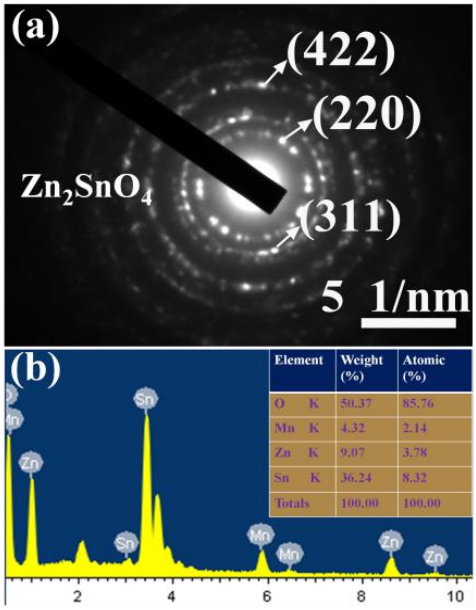


**Fig. S3** (a) The corresponding SAED pattern of $Zn_2SnO_4$ nanoneedle in the square area in Fig. 3b; (b) EDX spectrum of the final products (inset show the related data).

The corresponding cube-like selected-area electron diffraction (SAED) pattern was shown in Fig. S3a and the diffraction rings from the inside to outside of the pattern can be indexed to the (220), (311) and (422) planes of inverse spinel-type $Zn_2SnO_4$, respectively. From the results of EDX analysis (Fig. S3b), the mass fraction of Sn, Mn, Zn and O elements in the composites is about 36.24%, 4.32%, 9.07%, 50.37%, respectively. The mole ratio of Zn/Sn is 2.2, very close to the theoretical value of 2. In addition, from the results of the EDX, the mass content of $Mn_3O_4$ is about 6.00%.

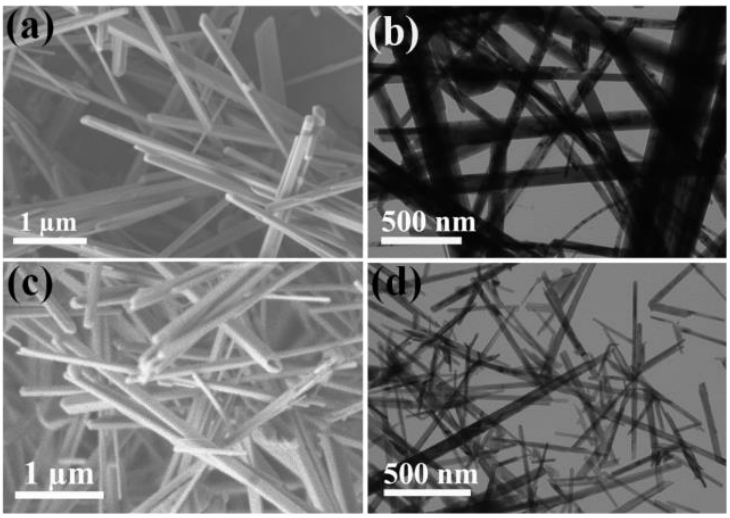


**Fig. S4** FESEM images of (a, c) branched MnOOH and as–prepared β-$MnO_2$ nanorods, respectively; (b, d) TEM images of the as-obtained MnOOH and β-$MnO_2$ nanorods, respectively.

It can be observed from Fig. S4a and S4b that most of the MnOOH particles display typical rod-like shapes and smooth surfaces, with diameters in the range of 80-200 nm and lengths of up to tens of micrometers. Fig. S4c and S4d display the SEM and TEM images of the as-obtained β-$MnO_2$, where the nanorods with smooth surface having an average diameter of 50 nm and lengths of up to 10 μm.

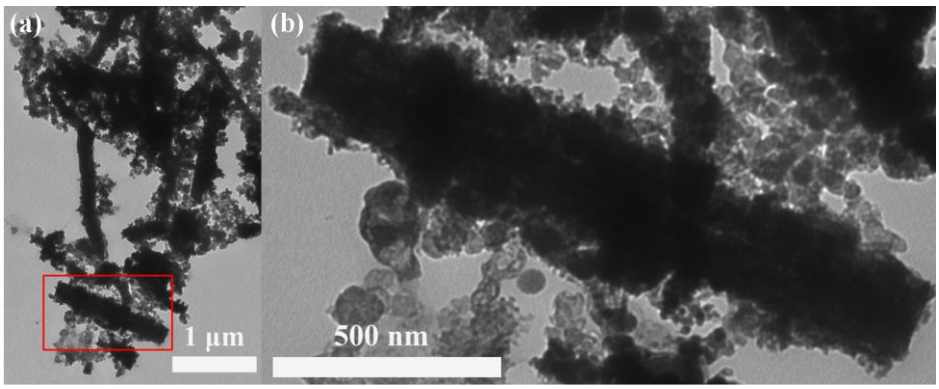


**Fig. S5** （a, b）TEM images of $Mn_3O_4/Zn_2SnO_4$/Li after 10 cycles at a current density of 1000 mA $g^{-1}$.

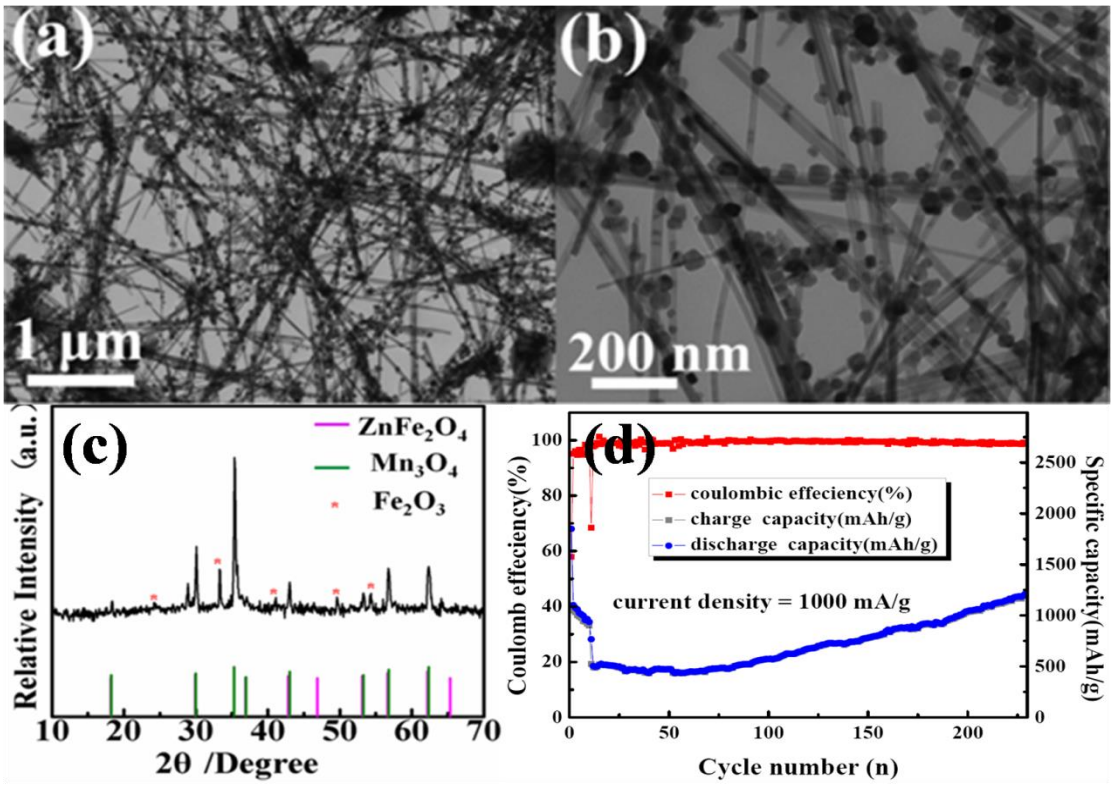


**Fig. S6** (a, b)TEM images and (c) XRD patterns of the 1D $ZnFe_2O_4/Mn_3O_4$ nanocomposites obtained after the hydrothermal process; (d) discharge/charge capacity and coulombic efficiency of the product at a current density of 1000 mA $g^{-1}$.

**Tab. S1** Cycle performance comparisons between the $Mn_3O_4$ /$ZnFe_2O_4$ composites and previously reported $ZnFe_2O_4$ structures.

| Materials | Reversible capacity (mAh/g) | Current density (mA/g) | Cycle number (n) | Ref. |
|---|---|---|---|---|
| $ZnFe_2O_4$/C hollow spheres | 625 | 500 | 30 | [1] |
| (Mg, Cu)co-doped $ZnFe_2O_4$ | 575 | 100 | 60 | [2] |
| $ZnFe_2O_4$ nanofibers | 733 | 60 | 30 | [3] |
| MWCNT–$ZnFe_2O_4$ | 1152 | 60 | 50 | [4] |
| $ZnFe_2O_4$/graphene | 600 | 200 | 90 | [5] |
| Our work ($ZnFe_2O_4$/ $Mn_3O_4$) | 1232.7 | 1000 | 230 | |

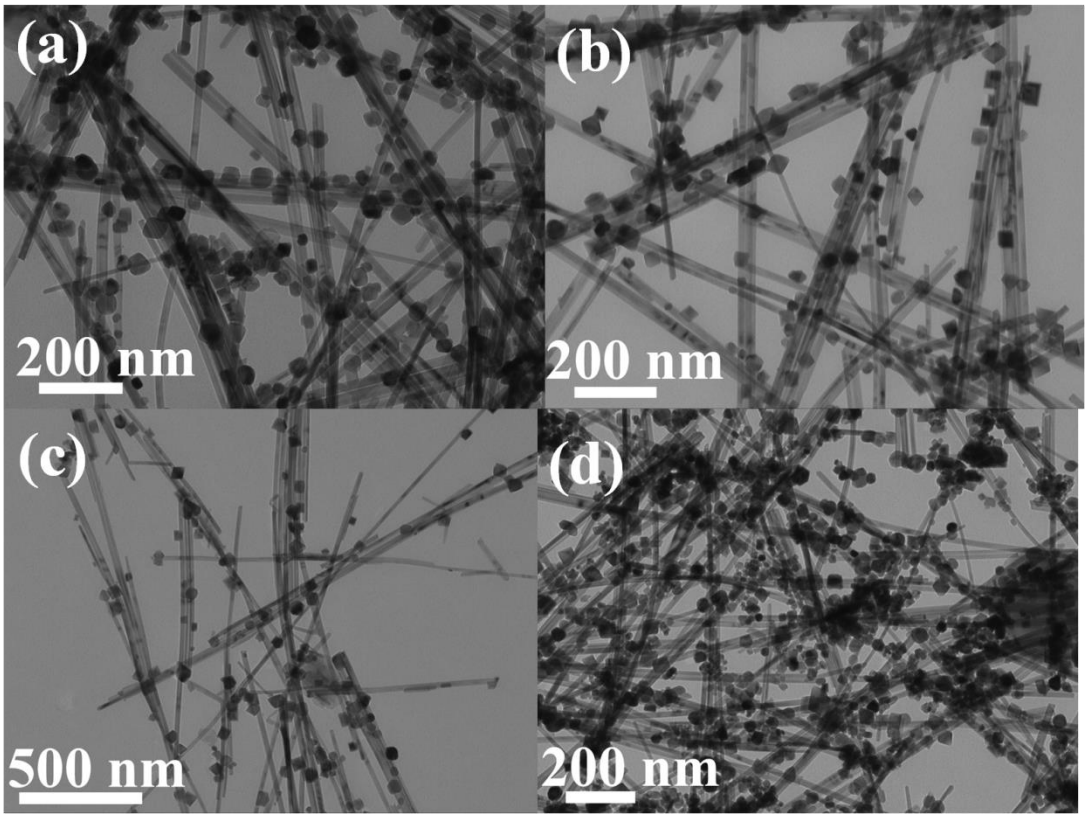


**Fig. S7** TEM images of the as-obtained 1D $ZnFe_2O_4/Mn_3O_4$ composites at 180°C/24 h using different amounts of urea: (a) 1.7 g, (b) 1.8 g, (c)1.9 g, and (d) 2.0 g.

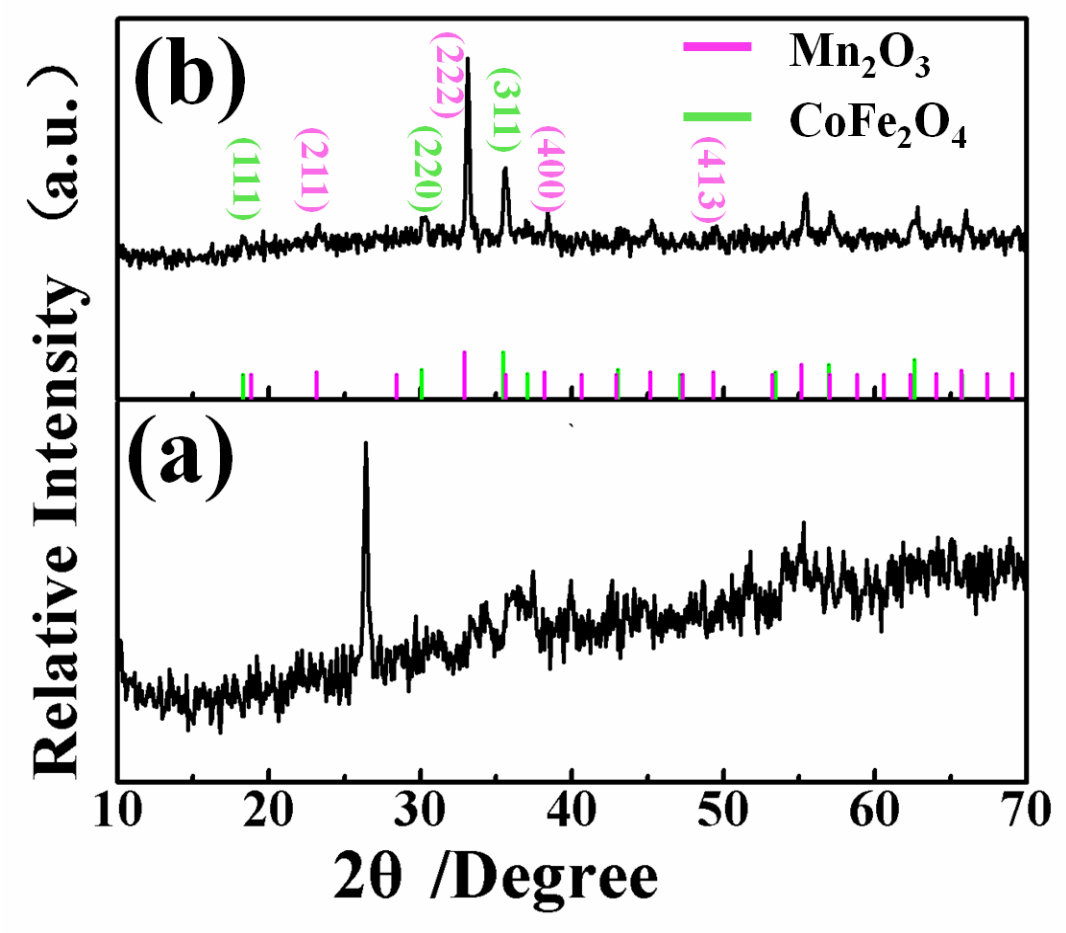


**Fig. S8** XRD patterns of (a) the black intermediate; (b) 1D $Mn_2O_3/CoFe_2O_4$ composites obtained after annealed at 620 °C in air for 2.5 h.

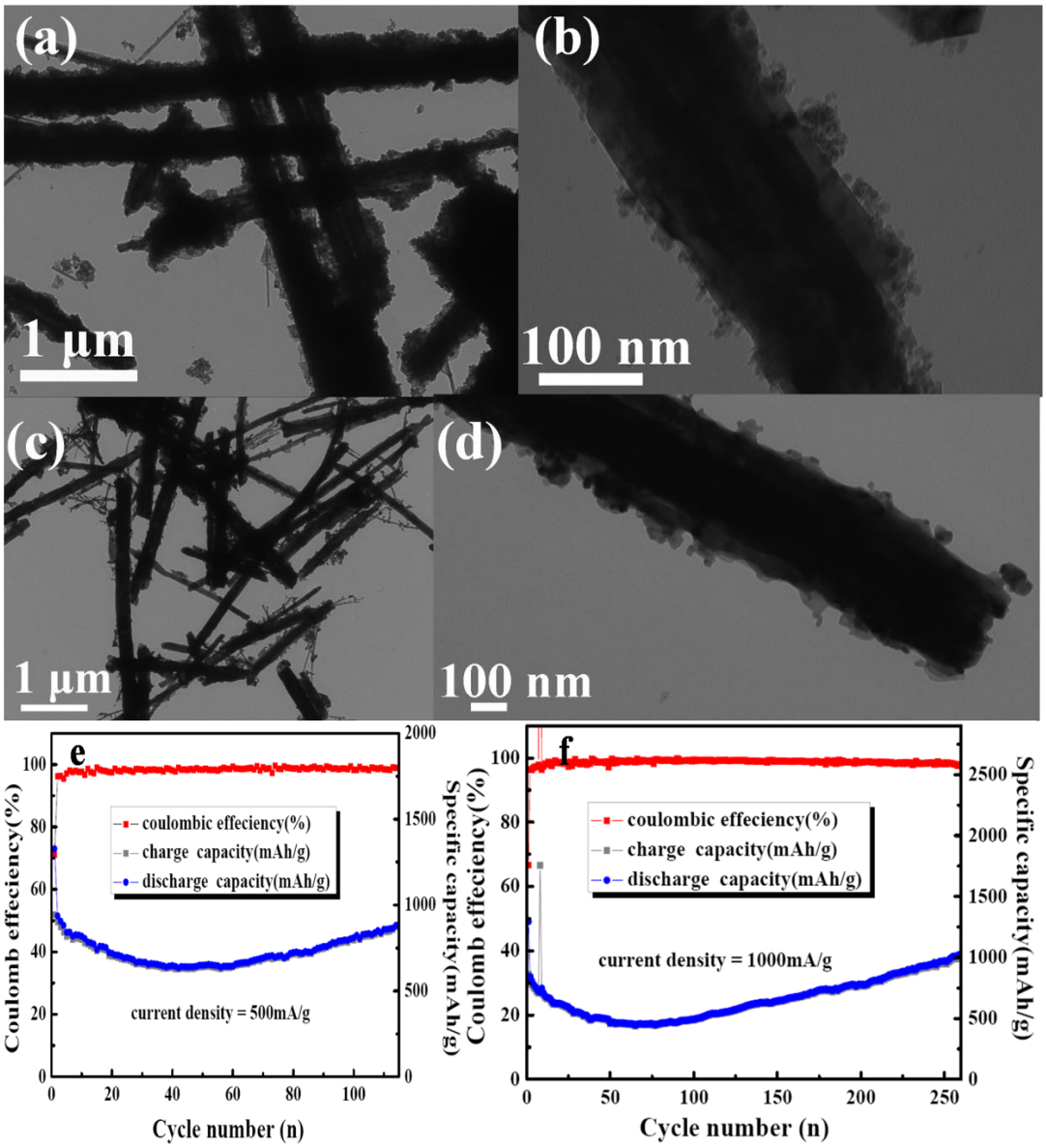


**Fig. S9** (a, b) TEM images of the black intermediate prepared at 180 °C for 24 h (8 mL $NH_3 \cdot H_2O$); (c, d) TEM image of 1D $Mn_2O_3/CoFe_2O_4$ composites obtained after annealed at 620 °C in air for 2.5 h; (e, f) discharge/charge capacity and coulombic efficiency of the $Mn_2O_3/CoFe_2O_4$ at a current density of 500 and 1000 mA $g^{-1}$, respectively.

**Tab. S2** Cycle performance comparisons between the $Mn_2O_3$ /$CoFe_2O_4$ composites and previously reported $ZnFe_2O_4$ structures.

| Materials | Reversible capacity | Current density | Cycle number | Ref. |
|---|---|---|---|---|

| | (mAh/g) | (mA/g) | (n) | |
|---|---|---|---|---|
| $CoFe_2O_4$/nitrogen-doped carbon | 646.2 | 0.1C | 80 | [6] |
| $CoFe_2O_4$/ rGO | 1040 | 0.1C | 30 | [7] |
| $Co_3O_4/CoFe_2O_4$ | 896.4 | 0.07C | 60 | [8] |
| $CoFe_2O_4$/graphene | 1082 | 100 | 50 | [9] |
| | 881.6 | 500 | 125 | |
| Our work ($Mn_2O_3$ /$CoFe_2O_4$) | 1008 | 1000 | 255 | |

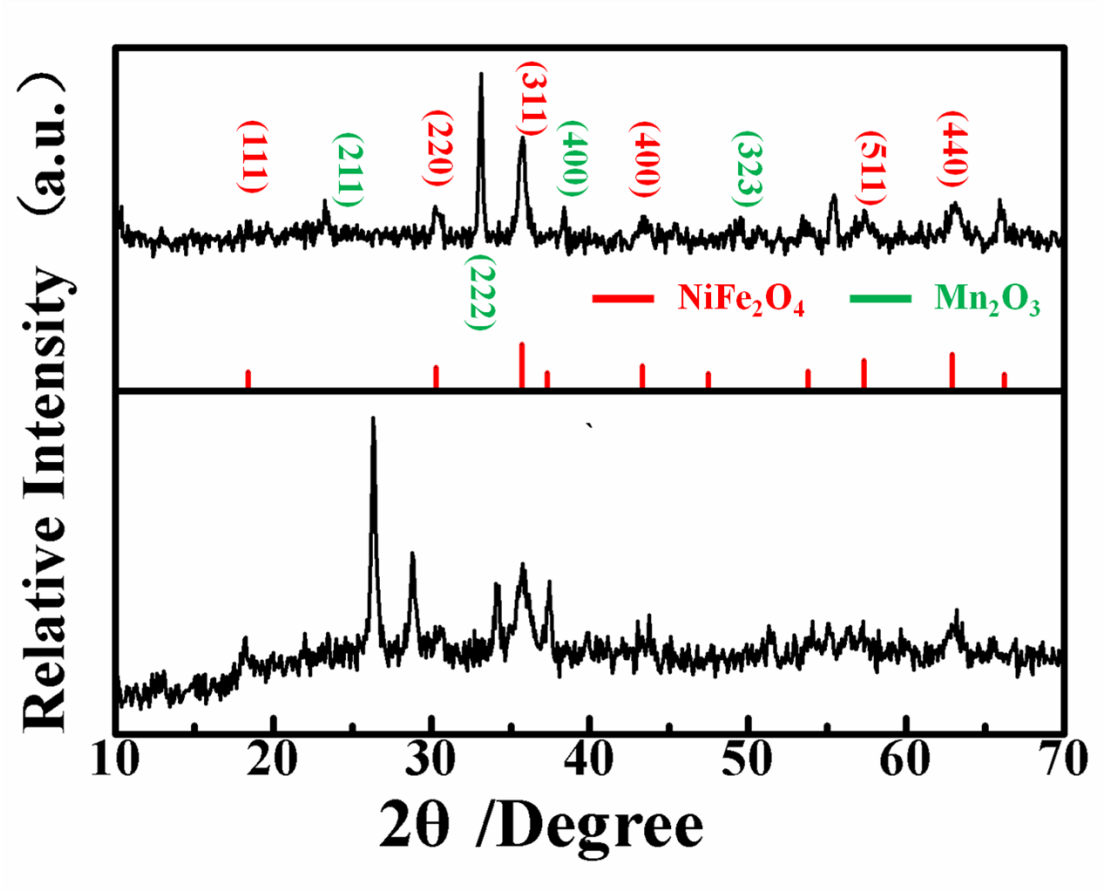


**Fig. S10** XRD patterns of a) the black intermediate ( 180 °C / 24 h ) ; b) 1D $Mn_2O_3/NiFe_2O_4$ composites obtained after annealed at 680 °C in air for 2.5 h.

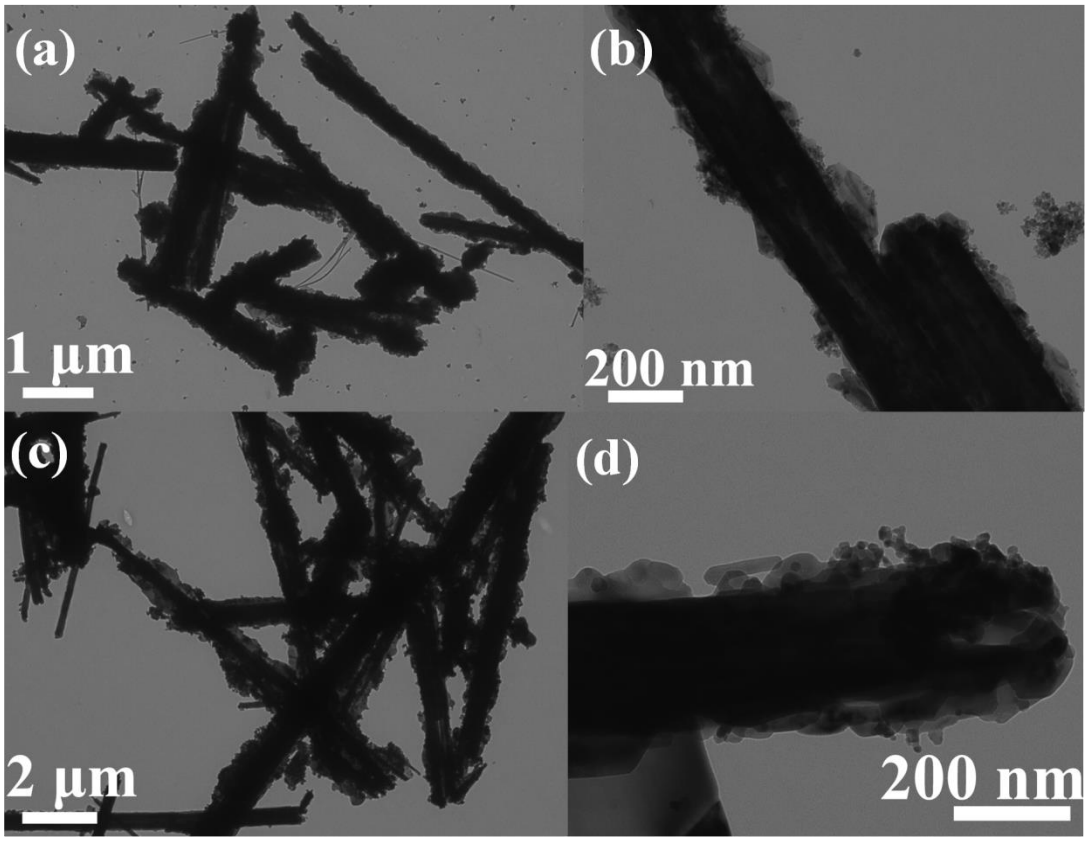


**Fig. S11** (a, b) TEM images of the black intermediate prepared at 180 °C for 36 h (8 mL$NH_3 \cdot H_2O$); (c, d) TEM image of 1D $Mn_2O_3/NiFe_2O_4$ composites obtained after annealed at 620 °C in air for 2.5 h.

## References


1. Y. F. Deng, Q. M. Zhang, S. D. Tang, L. T. Zhang, S. N. Deng, Z. C. Shi and G. H. Chen, *Chem. Commun*., 2011, **47**, 6828-6830.
2. A. S. Hameed, H. Bahiraei, M. V. Reddy, M. Z. Shoushtari, J. J. Vittal, C. K. Ong, and B. V. R. Chowdari, *ACS applied materials & interfaces*, 2014, **6**, 10744-10753.
3. P. F. Teh, Y. Sharma, S. S. Pramana and M. Srinivasan, *Journal of Materials Chemistry*, 2011, **21**, 14999-15008.
4. J. H. Sui, C. Zhang, D. Hong, J. Li, Q. Cheng, Z.G. Li and W. Ca , *Journal of Materials Chemistry*, 2012, **22**, 13674-13681.
5. W. T. Song, J. Xie, S. Y. Liu, G. S. Cao, T. J. Zhu and X. B. Zhao, *New J. Chem*, 2012, **36**, 2236–2241.
6. Z. J. Ding, B. Yao, J. K. Feng, J. X. Zhang, *Journal of Solid State Electrochemistry*, 2014**, 18**, 19-27.
7. P. R. Kumar, P. Kollu, C. Santhosh, K. E. V. Rao, D. K. Kim, A. N. Grace, *New Journal of Chemistry*, 2014, **38**, 2654-2661.
8. A. K. Rai, J. Gim, T. V. Thi, D. A., S. J. Cho, J. Kim, *The Journal of Physical Chemistry* C, 2014, **118**, 11234−1124.
9. H. Xi, D. D. Zhu, Y. S. Fu, X. Wang, *Electrochimica Acta*, 2012, **83**, 166-174**.**